



Kinematic Coregistration of Sentinel-1 TOPSAR Images Based on Sequential Least Squares Adjustment

Bing Xu , Zhiwei Li , Yan Zhu, Jiancun Shi, and Guangcai Feng 

Abstract—The Sentinel-1 provides an unprecedented opportunity for InSAR research and applications, especially in the field of fast and accurate damage assessment, thanks to its extra wide swath, short revisit interval, and free policy. Challenges also exist in Sentinel-1 terrain observation by progressive scans mode synthetic aperture radar (TOPSAR) interferometric processing, for example, the coregistration of TOPSAR images requires an accuracy of 0.001 pixels to reduce the phase jumps at the burst overlap region to 3°. To obtain the accuracy of 0.001 pixels for the coregistration of a stack of multitemporal TOPSAR images, joint estimation method and network-based method were proposed and implemented statically. However, when new images are added, the existing methods cannot coregister them kinematically. In order to resolve this issue, we first give a brief review for the existing static methods, including the single master-, temporally transferred-, and network-based methods, for coregistering multitemporal TOPSAR images. Then, we propose a kinematic coregistration method to coregister newly added TOPSAR images by introducing the sequential weighted least square adjustment. Experimental results demonstrate that the proposed method can achieve an accuracy of 0.001 pixels for kinematic coregistrations of multitemporal TOPSAR images. Compared with the static network-based coregistration method, the proposed method is superior in terms of both coregistration accuracy and computational efficiency. It will contribute a great deal to the globally acquired big SAR data (e.g., Sentinel-1 TOPSAR) and their near real-time processing.

Manuscript received September 27, 2019; revised February 12, 2020 and April 25, 2020; accepted May 26, 2020. Date of publication June 4, 2020; date of current version June 18, 2020. This work was supported in part by the National Natural Science Foundation of China under Grant 41804008, Grant 41474007, and Grant 41574005, in part by the National Science Fund for Distinguished Young Scholars under Grant 41925016, and in part by the National Key R&D Program of China under Grant 2018YFC1503603. (Corresponding author: Zhiwei Li.)

Bing Xu and Zhiwei Li are with the School of Geosciences and Info-Physics, Central South University, Changsha 410083, China, with the Key Laboratory of Metallogenic Prediction of Nonferrous Metals and Geological Environment Monitoring Ministry of Education, School of Geoscience and Info-Physics, Central South University, Changsha 410083, China, and also with the Hunan Key Laboratory of Nonferrous Resources and Geological Hazards Exploration, Changsha 410083, China (e-mail: xubing@csu.edu.cn; zwli@csu.edu.cn).

Yan Zhu and Jiancun Shi are with the School of Geosciences and Info-Physics, Central South University, Changsha 410083, China (e-mail: yanzhu@csu.edu.cn; jiancun.shi@csu.edu.cn).

Guangcai Feng is with the School of Geosciences and Info-Physics, Central South University, Changsha 410083, China, and also with the Key Laboratory of Metallogenic Prediction of Nonferrous Metals and Geological Environment Monitoring Ministry of Education, School of Geoscience and Info-Physics, Central South University, Changsha 410083, China (e-mail: fredgps@csu.edu.cn).

This article has supplementary downloadable material available at <http://ieeexplore.ieee.org>, provided by the authors.

Digital Object Identifier 10.1109/JSTARS.2020.3000043

Index Terms—Least squares adjustment, multitemporal terrain observation by progressive scans mode Synthetic Aperture Radar (TOPSAR) images coregistration, Sentinel-1, sequential weighted least square adjustment (SWLSA).

I. INTRODUCTION

THE terrain observation by progressive scans (TOPS) proposed by De Zan and Guarneri [1] was first implemented and validated by on-orbit satellites, including Radarsat-2 [2] and TerraSAR-X [3]–[7]. Meanwhile, a lot of theory analyses on TOPSAR (TOPS mode synthetic aperture radar) interferometric processing have been done [3]–[8]. New generation Sentinel-1A/-1B satellites provide wide-swath TOPSAR images, favorable for interferometric synthetic aperture radar (InSAR) research and applications. Particularly, Sentinel-1 provides an unprecedented opportunity for the fast and accurate damage assessment of natural disasters, which will improve the fast crisis response and understanding on disasters. However, great challenges exist in the InSAR data processing, for example, the coregistration of TOPSAR images requires an extremely high accuracy of 0.001 pixels [1], [4].

The coregistration of conventional strip-map mode synthetic aperture radar (SAR) images is based on the cross correlation of intensities (ICC) between two SAR images. In case of a long spatial baseline, the topographic relief will introduce additional local offsets, which will bias the affine transformation between images. Thus, the local offset shall be eliminated with an external digital elevation model (DEM) before using the ICC method for coregistration [9]. As reported, the ICC method could achieve an accuracy of up to 1/32 pixels [10], meeting the requirement of SAR interferometric processing of the strip-map mode data. Besides, the Doppler centroid of the SAR image of that mode is so small that the misregistration caused by the traditional ICC method is negligible.

Unlike traditional SAR satellites, Sentinel-1 acquires SAR data with the TOPS imaging mode that the azimuth beam electrically steers from the aft to the fore, resulting in a large linear Doppler centroid in the azimuth direction [1]. Consequently, a small misregistration could induce a rapidly changing phase ramp superimposed on interferograms of each burst. As a result, the interferometric phases on the overlap regions of consecutive bursts would be inconsistent and show as obvious phase jumps. For example, a misregistration of 1/32 pixels will cause a phase jump of about 90° for Sentinel-1 TOPSAR. Therefore,

for TOPSAR data processing, the misregistration becomes non-negligible. In order to reduce phase jumps on the burst overlap region to 3° , the coregistration accuracy should be 0.001 pixels. To meet the extremely high accuracy, the enhanced spectral diversity (ESD) method [3]–[8] was proposed, which determines the misregistration by the relationship between interferometric phase difference and spectral separation on the overlap region of adjacent bursts. The accuracy of the azimuth misregistration using the ESD method, however, is controlled by the coherence between the forward and backward looking interferograms that are exploited to obtain the interferometric phase difference on the overlap region. Therefore, when the ESD method is applied to coregister multitemporal Sentinel-1 SAR images under single master scenario [11] (SM-method), the temporal decorrelation will decrease the accuracy of the azimuth coregistration, especially in low-coherent areas. With the increasing time spans of image series, the coregistration errors under the SM-method constantly accumulate, resulting in large misregistrations. As a consequence, the multitemporal SAR images are not accurately coregistered mutually, and obvious phase jumps remain [12].

Regarding the coregistration of multitemporal Sentinel-1 TOPSAR, joint estimation-based [13], [14] and network-based methods [15] are proposed aiming at mitigating the azimuth coregistration errors by network adjustment [16]. Using these two methods, the multitemporal images are combined according to a given criterion, e.g., short temporal and spatial baseline [16], or n -connection [13], [15], and all the interferometric pairs are selected to construct a single network. Then, the ESD algorithm is exploited to estimate the coregistration offset of each selected pair in the network. Finally, the network adjustment is used to calculate the coregistration offsets for each slave image relative to the common reference image. For simplicity, we refer to this method as the network-based method (NB-method) in this study. Apart from the NB-method, Wegmüller *et al.* [17] proposed a method that uses the image-by-image transferring coregistration to reduce the effect of long time decorrelation, which is referred to as the temporally transferred method (TT-method) hereinafter. The TT-method uses a coregistered image as the reference to coregister the image with the shortest temporal baseline, and then exploits the ESD method to correct the misregistration of current interferometric pairs. Then, the coregistered image is used as the reference image to coregister the next image.

However, the NB- and TT-methods have their deficiencies. For the NB-method, it does not establish a scenario for kinematic multitemporal TOPSAR images coregistration. When new images added, all the previously coregistered multitemporal TOPSAR images shall be recoregistered together with the newly added images. The TT-method may alleviate the temporal decorrelation to some extent. However, coregistration offset errors in any previous coregistration propagate and accumulate, and finally bias the true offsets. Therefore, the TT-method does not solve the coregistration problem of multitemporal images.

In this study, we focus our attention on the kinematic coregistration for multitemporal TOPSAR images. By introducing the sequential weighted least square adjustment (SWLSA), we extend the static coregistration method into a kinematic one to

coregister newly added TOPSAR images. The article is organized as follows. Section II introduces the principle and existing methods of TOPSAR image coregistration. In Section III, the kinematic coregistration methods for multitemporal TOPSAR images are developed. Section IV presents the experimental validation of the proposed methods, followed by the comprehensive analysis and discussions in Section V. Finally, conclusions are drawn in Section VI.

II. EXISTING METHODS FOR MULTITEMPORAL SENTINEL-1 TOPSAR IMAGE COREGISTRATION

A. Principle of TOPSAR Coregistration

The antenna electronically steers from backward to forward when acquiring data in the TOPS mode, causing the Doppler centroid running through a relatively steep spectral ramp in each burst. As a consequence, a small coregistration error could introduce an azimuth phase ramp onto the interferogram for each burst. Thus, the interferometric phase with bias can be expressed as follows [5], [18]:

$$\phi = -\frac{4\pi}{\lambda}(r_M - r_S) + \phi_{\text{azerr}} \quad (1)$$

where r_M and r_S denote the range from radar to the same target in the master and slave acquisitions, respectively, and ϕ_{azerr} represents the phase bias, which can be expressed as follows [7], [18]:

$$\phi_{\text{azerr}}(t) = 2\pi f(t) \cdot \Delta t \quad (2)$$

where $f(t)$ is the Doppler centroid that varies linearly within a TOPS mode burst in the azimuth dimension, Δt is the azimuth misregistration in seconds. Assuming a constant azimuth misregistration for a single slice of TOPSAR dataset, we have $\Delta t = \Delta p \cdot dt$, with Δp denoting the azimuth misregistration in pixels, and dt the azimuth time interval in seconds. For simplicity, only a constant coregistration error [7], [8] is considered in this study. Since the Doppler centroid $f(t)$ changes rapidly and linearly within a single burst, even a very small coregistration error Δp may cause significant phase errors in the interferogram. Consequently, phase discontinuities or phase jumps inevitably manifest themselves in the burst overlap regions, see the example illustrated in Fig. 1. Such phase discontinuity can be expressed as follows:

$$\phi_{\text{sd}} = \phi_f - \phi_b \quad (3)$$

where ϕ_f and ϕ_b denote the forward and backward looking interferometric phases of the overlap region, respectively. Substituting (1) into (3) and considering the common InSAR phase observation equation $\phi = -4\pi(r_M - r_S)/\lambda = \phi_{\text{flat}} + \phi_{\text{topo}} + \phi_{\text{def}} + \phi_{\text{atm}} + \phi_{\text{noi}}$, we obtain the following:

$$\phi_{\text{sd}} = \Delta\phi_{\text{flat}} + \Delta\phi_{\text{topo}} + \Delta\phi_{\text{azdef}} + \Delta\phi_{\text{atm}} + \Delta\phi_{\text{noi}} + \Delta\phi_{\text{azerr}} \quad (4)$$

with

$$\Delta\phi_{\text{flat}} = \phi_{\text{flat},f} - \phi_{\text{flat},b}$$

$$\Delta\phi_{\text{topo}} = \phi_{\text{topo},f} - \phi_{\text{topo},b}$$

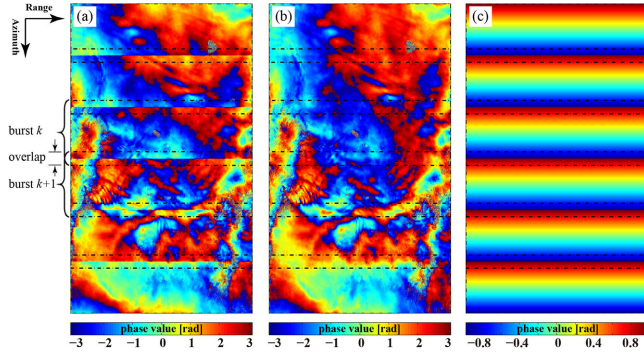


Fig. 1. Sentinel-1 TOPSAR image coregistered by the ESD method. (a) Original differential interferogram with the misregistration of 0.032 azimuth pixels. Due to the coregistration error, the overlap region of adjacent bursts (e.g., burst k and $k + 1$) shows obvious phase discontinuities. (b) Differential interferogram after applying the ESD method, in which the phase discontinuities are less obvious. (c) Simulated phase ramps for each burst using the misregistration estimated by the ESD method.

$$\begin{aligned}\Delta\phi_{\text{azdef}} &= \phi_{\text{def},f} - \phi_{\text{def},b} \\ \Delta\phi_{\text{atm}} &= \phi_{\text{atm},f} - \phi_{\text{atm},b} \\ \Delta\phi_{\text{noi}} &= \phi_{\text{noi},f} - \phi_{\text{noi},b} \\ \Delta\phi_{\text{azerr}} &= \phi_{\text{azerr},f} - \phi_{\text{azerr},b}\end{aligned}$$

where $\phi_{\text{flat},k}$, $\phi_{\text{topo},k}$, $\phi_{\text{def},k}$, $\phi_{\text{atm},k}$, and $\phi_{\text{noi},k}$ ($k=f, b$) represent the flat-earth phase, topographic phase, deformation phase, atmospheric phase, and noise phase in forward and backward looking geometries, respectively. $\Delta\phi_{\text{azdef}}$ is the azimuth deformation phase. $\Delta\phi_{\text{azerr}}$ denotes the phase difference in the overlap region caused by coregistration errors, which can be inferred from (2)

$$\Delta\phi_{\text{azerr}} = 2\pi \cdot \Delta f(t) \cdot \Delta p \cdot dt \quad (5)$$

where $\Delta f(t)$ is the Doppler centroid difference on the overlap region of consecutive bursts, representing the spectral separation. As the difference between the forward and backward looking geometries is so small that the phase differences for flat-earth, topographic component and atmospheric delay are always negligible, i.e., $\Delta\phi_{\text{flat}} \approx 0$, $\Delta\phi_{\text{topo}} \approx 0$ and $\Delta\phi_{\text{atm}} \approx 0$. Additionally, given that there is no azimuth displacement among the images to be coregistered, i.e., $\Delta\phi_{\text{azdef}} = 0$, (4) can be further simplified as follows:

$$\phi_{\text{sd}} \cong \Delta\phi_{\text{azerr}} + \Delta\phi_{\text{noi}}. \quad (6)$$

If the noise is neglected, i.e., $\Delta\phi_{\text{noi}} \approx 0$, $\Delta\phi_{\text{azerr}}$ could be replaced with ϕ_{sd} when estimating the azimuth coregistration offset Δp by (5)

$$\Delta p = \frac{\phi_{\text{sd}}}{2\pi \cdot \Delta f(t) \cdot dt}. \quad (7)$$

It is worth noting that ϕ_{sd} is modulo 2π , and the integer part could not be recovered. Thus, the ESD algorithm can only estimate the offsets corresponding to the non-integer part $[-\pi, \pi)$. For Sentinel-1 TOPSAR, the maximum estimable offset of the ESD algorithm is

$$\Delta p_{\text{max}} = \pm \frac{1}{2\Delta f_{\text{DC}}} \cdot \frac{1}{dt} \approx \pm 0.05 \text{ pixels} \quad (8)$$

where $\Delta f_{\text{DC}} = f_{\text{DC},f}(t) - f_{\text{DC},b}(t)$ represents the Doppler centroid difference between forward and backward looking on the overlap region of consecutive bursts.

As shown in (8), due to the phase ambiguity, the ESD algorithm has a prerequisite that the misregistration is smaller than 0.05 pixels. To meet this requirement, one can initiate the image coregistration using the orbit state vectors assisted with an external DEM (e.g., shuttle radar topography mission, SRTM), and refine the coregistration offset based on the intensity cross correlation to ensure the misregistration varying within ± 0.05 pixels [17], [19].

According to the error propagation law, as well as the relation between the coherence coefficient and the phase standard deviation [20], [21], and ignoring the covariance between the forward and backward looking interferograms, the accuracy of the estimated azimuth offset is

$$\sigma_{\Delta p} = \frac{\sqrt{2}\sigma_{\phi}}{2\pi \cdot \Delta f(t) \cdot dt} = \frac{1}{2\pi \cdot \Delta f(t) \cdot dt} \cdot \frac{1}{\sqrt{N_s}} \frac{\sqrt{1-\gamma^2}}{\gamma} \quad (9)$$

where N_s is the number of independent samples (that is the multi-look number applied to interferometric phase) and γ is the interferometric coherence.

B. Existing Methods

1) *Single-Master Coregistration Method*: The Single-Master coregistration method (SM-method) selects the optimal reference image based on temporal baselines, spatial baselines, and Doppler baselines [11], [16], then coregisters all slave images to the geometry of the reference image. Such a strategy can be applied to coregister multitemporal TOPSAR images. First, every interferometric pair is coregistered with the traditional SAR image coregistration algorithm, then the ESD algorithm estimates the misregistration by the forward and backward looking interferometric phase difference on the overlap region, which occupies 10% of the whole image [19]. However, the ESD is vulnerable to temporal decorrelation [22] in areas exposed to fast temporal decorrelation [14], [23], and the impact becomes significant with the temporal baseline increasing. In addition, the number of valid observations decreases dramatically, reducing the accuracy of ESD method or even leading to errors. Consequently, the offsets among any three images will be unclosed, which is the coregistration closure error.

2) *Temporally Transferred Coregistration Method*: To solve the effect of temporal decorrelation, especially the fast temporal decorrelation [23], Wegmüller *et al.* [17] proposed a strategy for coregistering TOPSAR images with available coregistered images, which is referred to as the TT-method in this article. It selects the temporally adjacent coregistered image as the reference image to reduce the temporal decorrelation. In the ESD algorithm [7], the coregistration accuracy is subject to the quality of the forward and backward looking interferometric phase difference on the burst overlap region. Therefore, the TT-method is to find an available coregistered image, and set it as the reference image. Such image shall have been coregistered with the common reference image and have the shortest temporal baselines relative to the image to be coregistered. Based on this, the first

image of the multitemporal TOPSAR images can be selected as the common reference image. Then slave images are coregistered one by one in chronological order, which are then successively transferred as the reference images for the ESD algorithm.

The revisit intervals are 12 days for both Sentinel-1A/B satellites, and are 6 days for the Sentinel-1 constellation. So, the TT-method can alleviate the effect of temporal decorrelation for the ESD algorithm to a certain extent. However, it is worth noting that any local coregistration error of the interferometric pairs would accumulate and propagate to subsequent images, which will be significant as the image amount increases and induce enclosure errors finally.

3) *Network-Based Coregistration Method*: The NB-method was first proposed by Hooper [16], aiming at bypassing the temporal decorrelation in coregistering long time strip-map SAR images. The NB-method estimates the image offsets for each interferometric pair in a short-baseline (spatial or temporal) network, then offsets relative to the common reference image are inverted by network adjustment with the offsets extracted previously. As the strip-map SAR image has relatively small Doppler centroid, the improvement in coregistration accuracy is not significant when the NB-method is used. However, for the coregistration of multitemporal TOPSAR images, the misregistration caused by temporal decorrelation is significant in the situation of rapidly changing Doppler centroid. To deal with such a problem, joint estimation methods [13], [14] and network-based methods [15] were proposed to estimate TOPSAR misregistration. This is similar to the Hooper's method [16]. First, a short-baseline network is established, then all TOPSAR images are coregistered by the traditional ICC coregistration method. The ESD algorithm is subsequently employed to estimate residual coregistration offsets for each image pair in the network. The precise misregistrations relative to the common reference image are finally obtained by the network adjustment.

Note that the NB-method does not have a unified network construction scheme. For the same image set, different thresholds of temporal or spatial baselines correspond to different networks. Besides, a large temporal threshold would increase the amount of image pairs in the network dramatically, causing a huge computation burden. In addition, the NB-method only provides solutions for the static coregistration of a set of multitemporal TOPSAR images, but cannot perform kinematic coregistration for newly added images.

III. NB AND SWLSA-BASED MULTITEMPORAL TOPSAR IMAGES COREGISTRATION METHOD

In this section, we divide image sets acquired in different phase into two parts, existing and newly added. First, we perform a coregistration method based on least squares adjustment for the coregistration of existing multitemporal images. Then, by introducing the SWLSA, we implement the kinematic coregistration of newly added images.

A. Network-Based Static Coregistration Method for Multitemporal TOPSAR Images

Given N TOPSAR images to be coregistered, for simplicity, we select the first image as the common reference. Note, the N

refers to the number of TOPSAR images, which is different from the N_s in (9). Actually, the common reference is always selected arbitrarily or via some optimal selection criterion [16]. In order to reduce error propagation, the series of images (sorted in chronological order) are combined to construct a short-baseline network, with M image pairs (or edges). The number of image pairs, M , satisfies the inequality

$$(N - 1) \leq M \leq \frac{N(N - 1)}{2}. \quad (10)$$

$M = (N - 1)$ is an extremely critical condition, which means 1-connection condition. In this condition, there are no redundant observations for error adjustment. Actually, M is greater than $N - 1$. Considering enough redundant observations and the lowest temporal decorrelation, the triangulation network is recommended, which means that each acquisition is connected to two following acquisitions (i.e., the 2-connections), then, $M = 2N - 3$.

Let us define the misregistration of each image pair (images i and j) in the triangulation network as $\Delta p_{i,j}$, with $i < j$ and $i, j \in [1, N]$. $\Delta p_{i,j}$ can be estimated by the ESD algorithm. Define the misregistrations of all images (including the reference image) relative to the common reference image as $\mathbf{X}_{all} = [x_{1,1}, x_{1,2}, x_{1,3}, \dots, x_{1,N}]^T$. Then, the relationships between the unknown parameters x_{all} and the observations $\Delta p_{i,j}$ can be expressed as follows:

$$\mathbf{L} = \mathbf{G}\mathbf{X}_{all} + \mathbf{e} \quad (11)$$

where \mathbf{G} is the design matrix with a size of $M \times N$, whose nonzero elements are given by $\mathbf{G}(k, i) = +1$ and $\mathbf{G}(k, j) = -1$, with k being the index of the image pair and $k \in [1, M]$. An example of the matrix form is provided as follows:

$$\mathbf{G} = \begin{bmatrix} -1 & +1 & 0 & 0 & \cdots & 0 \\ 0 & -1 & +1 & 0 & \cdots & 0 \\ -1 & 0 & +1 & 0 & \cdots & 0 \\ 0 & 0 & -1 & +1 & \cdots & 0 \\ \cdots & \cdots & \cdots & \cdots & \cdots & \cdots \end{bmatrix}. \quad (12)$$

Refer to Appendix A for the establishment of the design matrix. $\mathbf{L} = [\Delta p_{1,2}, \Delta p_{2,3}, \Delta p_{1,3}, \dots, \Delta p_{i,j}]^T$ is the observation vector with a size of $M \times 1$, \mathbf{e} is the error of observation vector.

The first image is set as the reference, that is, $x_{1,1} = 0$, which means the misregistration between the reference image and itself is zero. Thus, (11) can be written as (13) by removing the first column of matrix \mathbf{G} and the first element of \mathbf{X}_{all} , then

$$\mathbf{L} = \mathbf{A}\mathbf{X} + \mathbf{e} \quad (13)$$

where matrix \mathbf{A} is composed of columns 2 to N of matrix \mathbf{G} , and has a size of $M \times (N - 1)$. The unknown parameter vector is $\mathbf{X} = [x_{1,2}, x_{1,3}, \dots, x_{1,N}]^T$. Additionally, taking \mathbf{D} as the variance-covariance matrix of the observation \mathbf{L} , and $\mathbf{P} = \sigma_0^2 \mathbf{D}^{-1}$ as the weight matrix and ignoring the covariance between observations, we have $\mathbf{D} = \text{diag}(\sigma_{\Delta p_{1,2}}^2, \sigma_{\Delta p_{2,3}}^2, \dots, \sigma_{\Delta p_{i,j}}^2)$, where $\sigma_{\Delta p_{i,j}}^2$ can be calculated by (9). The unit weight variance σ_0^2 can be set to 0.001^2 pixels (the expected accuracy of coregistration). Rewriting (13) into the error equation, we obtain the following:

$$\mathbf{V} = \mathbf{A}\hat{\mathbf{x}} - \mathbf{l} \quad (14)$$

where $l = L - \mathbf{A}\mathbf{X}^0$, $\hat{\mathbf{x}} = \mathbf{X} - \mathbf{X}^0$, and \mathbf{X}^0 denotes the approximate value of parameter vector \mathbf{X} . According to the principle of weighted least squares, we obtain the following:

$$\hat{\mathbf{x}} = (\mathbf{A}^T \mathbf{P} \mathbf{A})^{-1} \mathbf{A}^T \mathbf{P} l. \quad (15)$$

Then, we can estimate the parameter vector $\hat{\mathbf{X}} = \mathbf{X}^0 + \hat{\mathbf{x}}$, corresponding to the azimuth misregistrations. The posterior variance factor is given by $\hat{\sigma}_0^2 = \frac{\mathbf{V}^T \mathbf{P} \mathbf{V}}{M - (N - 1)}$, and the posterior variance-covariance matrix of parameter vector is defined as $\mathbf{D}_{\hat{\mathbf{x}}} = \hat{\sigma}_0^2 (\mathbf{A}^T \mathbf{P} \mathbf{A})^{-1}$. The diagonal elements of $\mathbf{D}_{\hat{\mathbf{x}}}$ represent the variance of the estimated misregistration $\hat{\mathbf{X}}$.

B. Kinematic Coregistration Method for Newly Added TOPSAR Images

In this section, we combine the existing image sets with newly added images and implement the kinematic coregistration of two TOPSAR image sets by introducing the SWLSA. Given two sets (S_1 and S_2) of TOPSAR images acquired in two different phases, with N_1 and N_2 images, respectively. The first image in S_1 is selected as the reference image. Let the observation vectors be \mathbf{L}_1 and \mathbf{L}_2 , and the unknown vectors be $\mathbf{X}_a = [x_{12}, x_{13}, \dots, x_{1N_1}]^T$ and $\mathbf{X}_b = [x_{1N_1+1}, x_{1N_1+2}, \dots, x_{1N_2}]^T$, respectively. Then, the observation equations of the two sets are

$$\mathbf{L}_1 = \mathbf{A}_1 \mathbf{X}_a + e_1 \text{ with weight matrix } \mathbf{P}_1 \quad (16)$$

$$\mathbf{L}_2 = \mathbf{A}_2 \mathbf{X}_a + \mathbf{B}_2 \mathbf{X}_b + e_2 \text{ with weight matrix } \mathbf{P}_2 \quad (17)$$

where \mathbf{X}_a is the vector of the common unknown parameters, \mathbf{X}_b is the newly added unknown parameters after extending the triangulation network to incorporate more (the newly added) multitemporal TOPSAR images. For details of the establishment of the design matrices \mathbf{A}_1 , \mathbf{A}_2 , and \mathbf{B}_2 , refer to Appendix B. The two images sets are processed separately, since they are not simultaneously acquired. First, S_1 acquired in Phase I is coregistered with the proposed static coregistration method

$$\hat{\mathbf{x}}'_a = (\mathbf{A}_1^T \mathbf{P}_1 \mathbf{A}_1)^{-1} \mathbf{A}_1^T \mathbf{P}_1 l_1 \quad (18)$$

$$\mathbf{D}_{\hat{\mathbf{x}}'_a} = \frac{\mathbf{V}_1^T \mathbf{P}_1 \mathbf{V}_1}{M_1 - (N_1 - 1)} (\mathbf{A}_1^T \mathbf{P}_1 \mathbf{A}_1)^{-1} \quad (19)$$

$$\hat{\mathbf{X}}'_a = \mathbf{X}_a^0 + \hat{\mathbf{x}}'_a. \quad (20)$$

Then, the images of S_2 acquired in Phase II are coregistered to the reference image in S_1 . As the images in S_1 have been coregistered, these coregistration results [obtained with (18)–(20)] shall be taken into consideration for the coregistration of S_2 . Using SWLSA [24] and taking the previous adjustment results of S_1 (18)–(20) as the priori information, we establish the pseudo-observation equation

$$\begin{aligned} \mathbf{V}_{\hat{\mathbf{x}}'_a} &= \mathbf{I} \hat{\mathbf{x}}''_a \text{ with weight matrix} \\ \mathbf{P}_{\hat{\mathbf{x}}'_a} &= \mathbf{A}_1^T \mathbf{P}_1 \mathbf{A}_1 \end{aligned} \quad (21)$$

where \mathbf{I} is an identity matrix with a size of $(N_1 - 1) \times (N_1 - 1)$, and $\hat{\mathbf{x}}''_a$ are the unknowns. Besides, taking $\hat{\mathbf{X}}'_a = \mathbf{X}_a^0 + \hat{\mathbf{x}}'_a$ as the initial value of \mathbf{X}_a , and \mathbf{X}_b^0 as the initial value of \mathbf{X}_b , and

substituting them into (17), we obtain the corresponding error equation

$$\mathbf{V}_2 = \mathbf{A}_2 \hat{\mathbf{x}}''_a + \mathbf{B}_2 \hat{\mathbf{x}}_b - \bar{l}_2 \text{ with weight matrix } \mathbf{P}_2 \quad (22)$$

where $\bar{l}_2 = -(\mathbf{A}_2 \hat{\mathbf{X}}'_a + \mathbf{B}_2 \mathbf{X}_b^0 - \mathbf{L}_2)$. Combining (21) and (22), the error equations can be rewritten as follows:

$$\begin{aligned} \begin{bmatrix} \mathbf{V}_{\hat{\mathbf{x}}'_a} \\ \mathbf{V}_2 \end{bmatrix} &= \begin{bmatrix} \mathbf{I} & \mathbf{0} \\ \mathbf{A}_2 & \mathbf{B}_2 \end{bmatrix} \begin{bmatrix} \hat{\mathbf{x}}''_a \\ \hat{\mathbf{x}}_b \end{bmatrix} - \begin{bmatrix} \mathbf{0} \\ \bar{l}_2 \end{bmatrix} \\ \text{with weight matrix} & \begin{bmatrix} \mathbf{P}_{\hat{\mathbf{x}}'_a} \\ \mathbf{P}_2 \end{bmatrix} \end{aligned} \quad (23)$$

By the weighted least squares adjustment, we obtain the estimate of the parameters

$$\begin{bmatrix} \hat{\mathbf{x}}''_a \\ \hat{\mathbf{x}}_b \end{bmatrix} = \begin{bmatrix} \mathbf{A}_1^T \mathbf{P}_1 \mathbf{A}_1 + \mathbf{A}_2^T \mathbf{P}_2 \mathbf{A}_2 & \mathbf{A}_2^T \mathbf{P}_2 \mathbf{B}_2 \\ \mathbf{B}_2^T \mathbf{P}_2 \mathbf{A}_2 & \mathbf{B}_2^T \mathbf{P}_2 \mathbf{B}_2 \end{bmatrix}^{-1} \begin{bmatrix} \mathbf{A}_2^T \mathbf{P}_2 \bar{l}_2 \\ \mathbf{B}_2^T \mathbf{P}_2 \bar{l}_2 \end{bmatrix}. \quad (24)$$

Then, the final parameter vectors (the azimuth misregistrations of all images) can be estimated by

$$\hat{\mathbf{X}}''_a = \hat{\mathbf{X}}'_a + \hat{\mathbf{x}}''_a = \mathbf{X}_a^0 + \hat{\mathbf{x}}'_a + \hat{\mathbf{x}}''_a \quad (25)$$

$$\hat{\mathbf{X}}_b = \mathbf{X}_b^0 + \hat{\mathbf{x}}_b. \quad (26)$$

It follows that the adjustment results of S_1 are taken as the priori information in coregistering S_2 . And its coregistration offsets are updated to achieve a high coregistration accuracy during the coregistration of S_2 , see (25).

IV. EXPERIMENTS

A. Dataset and Preprocessing

To validate the kinematic multitemporal TOPSAR image coregistration method, we select Mexico City as the experimental area, which processes a large number of TOPSAR images and has been used for validating TOPS imaging mode with TerraSAR-X [6] and Radarsat-2 [2] satellites. The experimental data consist of 101 TOPSAR images acquired on track 143 from November 8, 2014 to July 13, 2017, with a time span of 978 days (see Table S1 in Supplementary A for details). Nearly 2/3 of the area is either vegetation-covered or decorrelated, so it is well suited to test the validity of an algorithm in the long-time decorrelation area. In this study, the proposed methods, as well as existing coregistration methods for multitemporal TOPSAR images, including SM-method, TT-method, and NB-method, are tested and compared. For simplicity, six bursts on subswath 3 are processed in the experiment. The data coverage and corresponding mean intensity image are shown in Fig. S1 in Supplementary A.

In data processing, the first image, acquired on November 8, 2014, is selected as the reference image. Before estimating the misregistration of TOPSAR images by the ESD algorithm, the images shall be coregistered to limit the offsets within ± 0.05 pixels [17], [19]. Such a process can be implemented by the traditional ICC coregistration method, assisted by the orbit state vectors and external DEM (e.g., SRTM DEM), to correct the local topography induced image offset. And such a process could be easily accomplished by sophisticated InSAR data processing

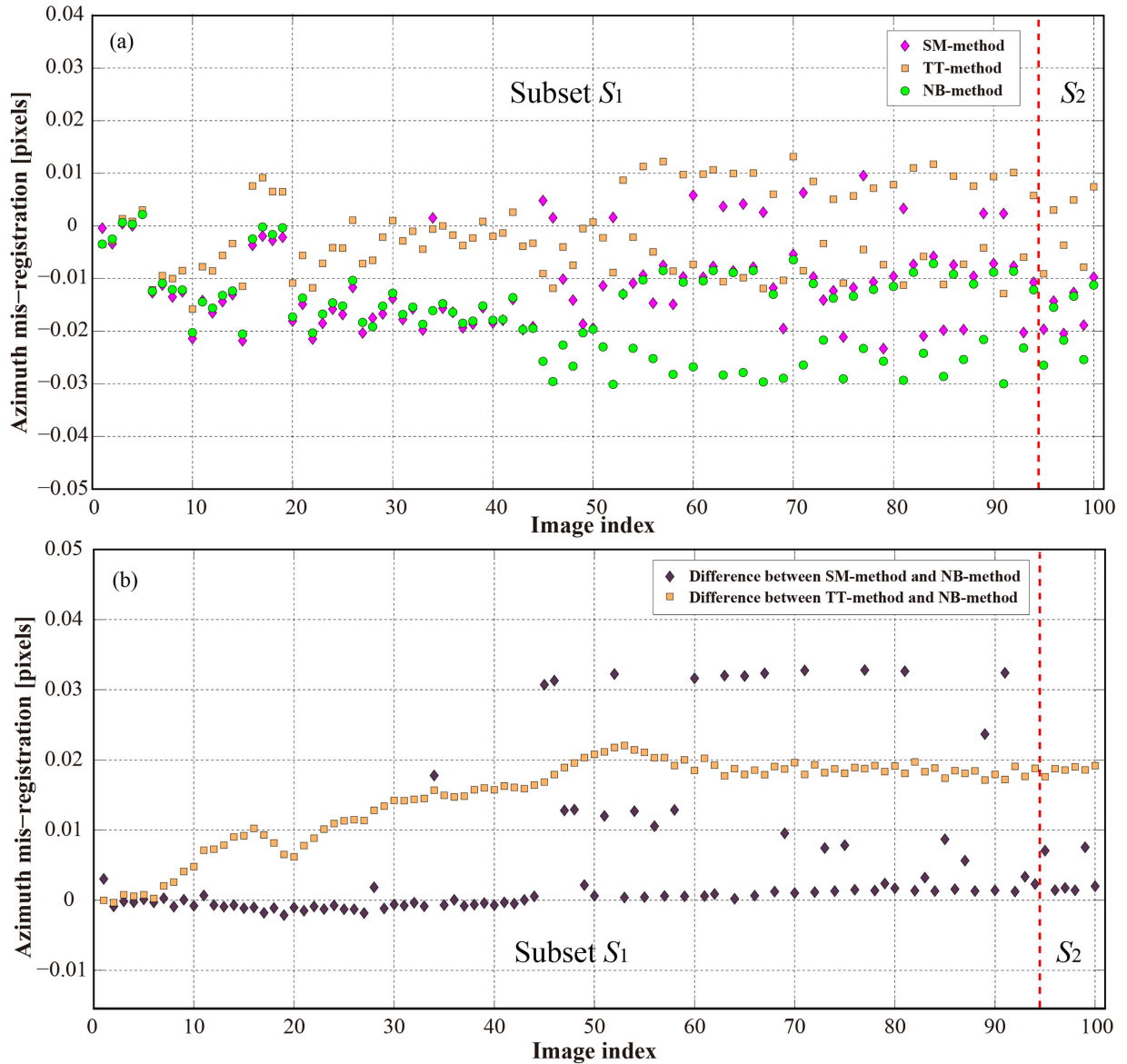


Fig. 2. Static coregistration results. (a) Estimated misregistrations of the SM-method, TT-method, and NB-method. (b) Comparison of misregistration between NB-method and other two methods (SM-method and TT-method). The results of NB-method is taken as the reference. The black diamonds denotes the difference between the results of SM-method and NB-method, and orange rectangle denotes the difference between TT-method and NB-method.

software, such as GAMMA [17] and GMTSAR [25]. We do not discuss this specific implementation because it is out of the scope of our study.

Subsequently, the misregistrations (residual offsets) are estimated by the multitemporal TOPSAR images coregistration methods, including the SM-method, TT-method, and NB-method, as well as the proposed method.

B. Static Coregistration

In order to make a reliable comparison, we first coregister all 101 TOPSAR images by treating them as only one set of images. The TT-method, SM-method, and NB-method are respectively exploited to get the static coregistration results, which are shown in Fig. 2(a). We can see that the three results are different from each other. As manifested in the previous articles [13], [15],

the NB-method can coregister a single set of multitemporal TOPSAR images. Because the NB-method uses a network for coregistration error adjustment, we can use the root mean square error (RMSE) of the residual errors from the adjustment. The RMSE for NB-method is 1.11×10^{-3} pixels, demonstrating that the NB-method has a high accuracy for coregistering multitemporal TOPSAR images.

To evaluate the performance of SM- and TT-methods, we select the result of NB-method as reference and calculate the differences [see Fig. 2(b)] among the results in Fig. 2(a). It shows that, within a short time period (image index < 30), the SM-method has few errors. However, the errors become large and random with the time span increasing. For the TT-method, the errors propagate and accumulate continuously as time goes on, showing an obvious trend. Based on these analyses, we believe that both SM- and TT-methods cannot meet the requirement for

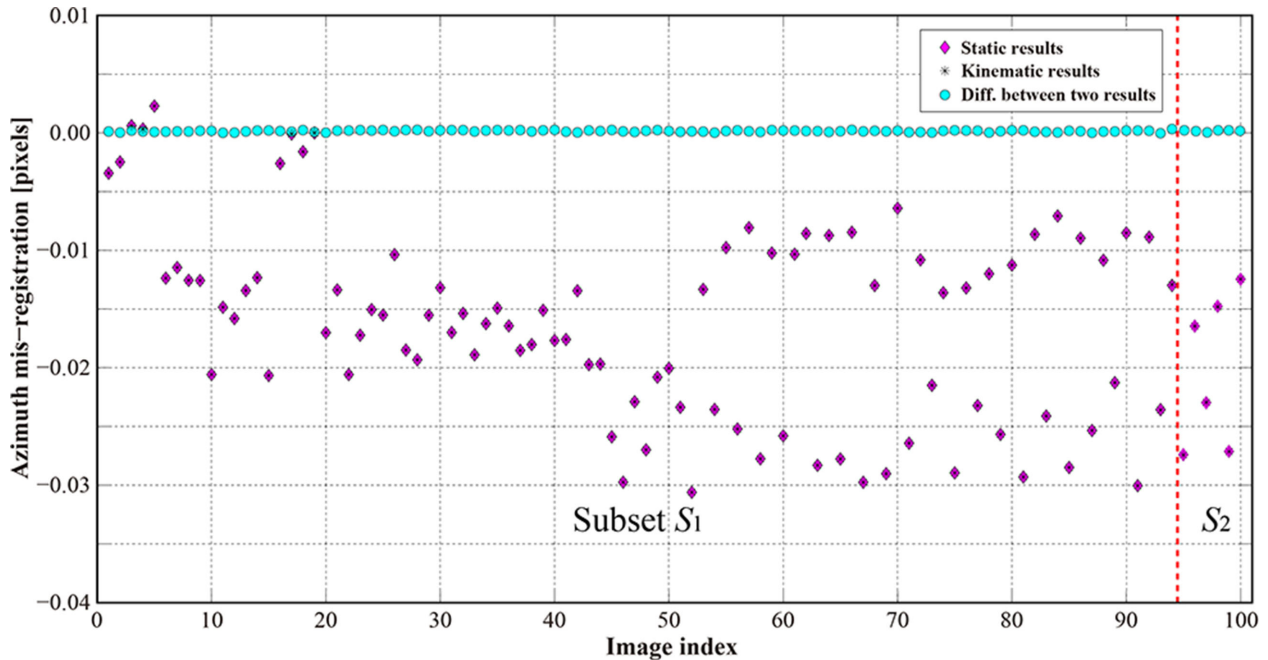


Fig. 3. Comparison between the static coregistration and kinematic coregistration. The red dash line divides the image series into two sets, S_1 (left) and S_2 (right). The purple diamonds denote the static coregistration results, the black stars denote the kinematic coregistration results, the cyan dots denote the difference of the two results, corresponding to \hat{x}'_a in (25).

coregistering multitemporal TOPSAR images. Therefore, we do not discuss SM- and TT-methods, and the NB-method is selected as static method in subsequent analysis.

C. Kinematic Coregistration of Newly Added TOPSAR Images

The first 95 images, indexing from 1 to 95 with a time span of 942 days, compose S_1 for the coregistration experiment. And the rest 6 images are treated as the newly added TOPSAR images, acquired on the same coverage with S_1 , to form S_2 that shall be coregistered to the reference image of Subset S_1 .

The NB-method, however, has no available kinematic coregistration scheme. Thus, the newly added images (S_2) shall be combined with S_1 to form one set and be coregistered by the static coregistration scheme. For the NB-method, all possible interferometric pairs could be exploited to form the network theoretically. However, the ESD algorithm is affected by the temporal decorrelation, which shall be considered in selecting interferometric pairs for the network construction. In order to construct a reasonable short-baseline network with consideration of computational efficiency, we set the temporal baseline threshold as 36 days, which is 3 times of the revisit interval of Sentinel-1 satellite. Under the circumstances, the mean coherence remains at the level of 0.75 (see Supplementary B). And the spatial baseline threshold is set as 150 m, 1.5 times of the Root Mean Square (100 m) of the Sentinel-1 orbital tune diameter [26]. Then, a short-baseline network consisting of 367 interferometric pairs is established. Furthermore, the misregistration of each interferometric pair in the network is estimated by the ESD algorithm. After getting all the misregistrations, the misregistrations of all the slave images relative

to the common reference image (index 1) are inverted by the network adjustment.

The proposed method can simply implement the kinematic coregistration, see details in Section III-B. Specifically, the images in S_1 are coregistered via the static coregistration process, see (18)–(20). The coregistration results are taken as the priori information for the triangulation adjustment of the coregistration of S_2 , which can avoid unnecessary repeated coregistration process. Then, we construct the short-baseline network with the images in S_2 , and calculate the misregistrations referring to (24)–(26). Consequently, the kinematic coregistration is implemented for the newly added images.

1) *Coregistration Results*: Fig. 3 shows the misregistration results when new images are added, see the right part of the red dashed line. For the static method, all images have to be coregistered by reconstructing a new network when new images are added. While for the proposed method, the coregistration results of S_1 are considered as the priori information for the adjustment of the second coregistration, and simultaneously get updated [see (25)] to obtain the optimal coregistration.

Additionally, the RMSE of the residual errors from the adjustment for both the static method and the proposed method are 1.11×10^{-3} pixels and 1.02×10^{-3} pixels, respectively, indicating that the two methods have achieved high-precision coregistration. And the accuracy of the proposed method is 8.1% higher than that of the static method.

For the static method, when new images are added, all images including the coregistered ones must be recoregistered. Nevertheless, the proposed method takes the previous results as the priori information for the error adjustment, rather than to repeatedly estimate the offsets of the former coregistered images in S_1 with the ESD algorithm.

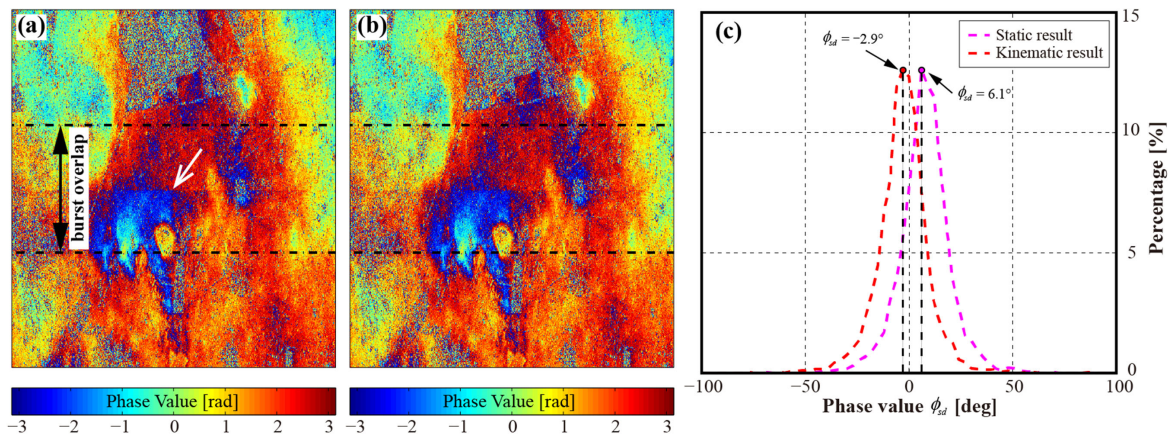


Fig. 4. Phase jump error check results. Interferograms generated by two images (acquired on June 7, 2017 and July 7, 2017) that were coregistered by (a) static method, and (b) kinematic method; (c) histogram statics of phase differences between the forward and back interferogram on the burst overlap region. The purple dotted line denotes the result of static method, and the red dotted line denotes the results of the kinematic method. The circles are the histogram extreme values, and the corresponding phase values represent the level of coregistration accuracy. The smaller the value, the higher the coregistration accuracy.

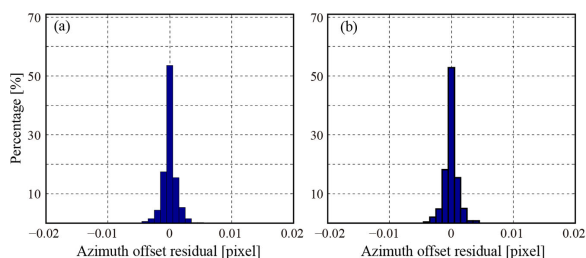


Fig. 5. Statistical histograms of residual offsets of (a) the static method and (b) the kinematic method.

TABLE I
RESIDUAL ERRORS FOR THE TWO METHODS

Methods	RMSE (pixels)	MAE (pixels)	Errors within $\pm 10^{-3}$ pixels (%)
static method	1.10×10^{-3}	0.83×10^{-3}	72.7
our method	1.02×10^{-3}	0.71×10^{-3}	78.4

For the kinematic coregistration after adding new images, the coregistration offsets of S_1 is updated, see the updated value \hat{x}''_a in (25). We calculate the difference between static and kinematic coregistrations. The results in Fig. 3(a) (cyan dots) show that the value of correction \hat{x}''_a ($< 0.5 \times 10^{-3}$) is too small to be considered.

2) *Phase Jump Error Check*: If multitemporal TOPSAR images are precisely coregistered, the residual offsets for any interferometric pair would be zero. We select two images, acquired on June 7, 2017 and July 7, 2017 from S_1 and S_2 , respectively, to generate interferogram and analyze the enclosure error of coregistering images, see Fig. 4. We can see that The NB-method has suspected phase jump [see the white arrow in Fig. 4(a)]. For the proposed method, the burst overlap area [see Fig. 4(b)] also shows a slight phase jump. However, the phase jump of the static result is more significant than the kinematic one.

Furthermore, we conduct histogram statistics on the phase difference of the forward and backward looking interferometric phase on the overlap region (see Fig. 4). The residual offset is proportional to the statistic mean value, see (5). The mean value of the static result is 6.1° , showing a relatively apparent phase jump. While the equivalent of kinematic result is much smaller, which is -2.9° , demonstrating a higher accuracy. In particular, the phase value ϕ_{sd} of kinematic result is within the range of $\pm 3^\circ$, which means the kinematic method can coregister multi-temporal TOPSAR images with high accuracy.

V. ANALYSIS AND DISCUSSION

In order to achieve an accuracy better than 0.001 pixels, we propose a kinematic method for multitemporal TOPSAR images by introducing the SWLSA. Here, we make a comprehensive comparison between the proposed method and static method, as well as discussions concerning the results.

A. Comparisons of Coregistration Accuracies

The coregistration accuracy could be assessed by the RMSE of residual errors in observation vectors for the static method or our method. For our method, the kinematic coregistration accuracy is 1.02×10^{-3} pixels after adding six new images. While the RMSE for the static method is 1.11×10^{-3} pixels. It is 8.1% higher than that of the NB-method.

Furthermore, if all images have been coregistered to a common reference image, the residual offset of any two images would be zero, and the nonzero value indicates misregistration. Thus, in this case, we can evaluate the coregistration accuracy by reestimating the image residual offsets with the ESD algorithm. Theoretically, any interferometric pairs could be employed for accuracy evaluation. However, the accuracy of the ESD algorithm is affected by decorrelation, as explained in Section II. To avoid the temporal decorrelation, interferometric pairs with a temporal baseline smaller than 60 days are selected, which ensures the mean coherence larger than 0.7, see Supplementary

TABLE II
 CUNSUMED TIME OF THE TWO METHODS FOR COREGISTERING SIX NEWLY ADDED TOPSAR IMAGES

Methods	Network Scenario	Number of Pairs to Apply ESD	ESD Consuming Time ¹ (s)	Resampling Consuming Time ² (s)	Total Consuming Time ³ (s)
Static Method	2-connections	199	$34.2 \times 199 = 6805.8$	$53.6 \times 100 = 5360$	12165.8
Kinematic Method	2-connections	12	$34.2 \times 12 = 410.4$	$53.6 \times 6 = 321.6$	732.0

¹Consumed time of ESD = consumed time of one interferometric pair \times number of interferometric pairs.

²Consumed time for resampling = consumed time of one SLC resampling \times number of SLC images to be resampled.

³Total consumed time = consumed time of ESD + consumed time of resampling.

B for details. We obtain 545 interferometric pairs, and then estimate their residual offsets using the ESD algorithm. Histograms of these residual offsets are subsequently computed. As Fig. 5 shows, the coregistration residual offsets of the four methods are mostly within the range of $[-0.001, 0.001]$ pixels, with a few outside the range, and some even outside the range of $[-0.005, 0.005]$ pixels. Note that the errors of the proposed method and NB-method are concentrated around zero.

The accuracy is further accessed by the RMSE, the mean absolute error (MAE), and the percentage of the errors within $\pm 10^{-3}$ pixels of the residual offsets. The results listed in Table I show that, among the 545 interferometric pairs, the percentages of residual offsets within $\pm 10^{-3}$ pixels for these two methods are respectively 78.4% and 72.7% for our method and the NB-method, indicating high accuracies. The accuracy of our method is even higher than that of the static method. Besides, the RMSE and MAE for the NB-method are 1.10×10^{-3} pixels and 0.83×10^{-3} pixels, respectively. And the equivalents of our method are 1.02×10^{-3} pixels and 0.71×10^{-3} pixels, respectively, showing improvements of 7.3% and 14.5% over the static method, respectively. The results demonstrate that the images have been coregistered by our method with an accuracy of 0.001 pixels. We shall bear in mind that, the previous static coregistration results of the 95 images are taken as prior information for the error adjustment in kinematic coregistration. Therefore, we believe that the improvement of kinematic results over the static results is reliable.

B. Evaluation of the Computation Performance

Currently, the Sentinel-1A and -1B satellites have already run on orbit, and they share one orbital plane with an orbital cycle phase difference of 180° . The revisit interval is 12 days for a single satellite, while 6 days for the combination of Sentinel-1A and -1B satellites. With such a high time resolution, unnecessary repeat coregistration will dramatically increase the computational burden and the efficiency of the whole process will decrease.

We compare the computational performance of the static and kinematic methods, in terms of the elapsed time for kinematically coregistering the newly added six TOPSAR images, see Table II. For the static method, the previous coregistered 95 images shall be recoregistered together with the newly added 6 images. While for the kinematic method proposed in the

article, only the newly added images shall be coregistered. For a reasonable comparison, we assumed two-connections network construction scenario for both static and kinematic methods. Besides, we assumed that images of Subset S_1 have already been coregistered.

For the static method, when new images are added, the static method shall recoregister both new and old images together. Thus, 199 times of ESD and 100 times of Single Look Complex (SLC) image resampling shall be performed to coregister the 101 TOPSAR images. The total consuming time is about 12165.8 s. While kinematic method only needs to estimate the coregistration offsets of the extended network of the newly added images and resample the new images. And the total consuming time is only 732.0 s. Therefore, the computational efficiency is obviously higher.

At present, satellites Sentinel-1A and -1B have systematically acquired TOPSAR image data with a short revisit interval, allowing the systematical and periodical geological disaster monitoring. However, processing such big SAR data is a great challenge, especially when the near real-time data processing is needed. The proposed kinematic method for multitemporal TOPSAR images coregistration method giving new idea for TOPSAR data near real-time processing.

C. Potential Error Sources

According to the ESD algorithm (see section II-A), the misregistration is estimated based on the difference of forward and backward looking interferometric phases on the burst overlap region. It implies two assumptions: first, the difference between the two looking geometries is small, so that the flat earth phase and topographic phase of corresponding interferometric pairs can be cancelled out; second, the deformation along the azimuth direction is zero or can be ignored. If the assumptions were satisfied, the random phase noise would be the only error source affecting the estimation of misregistration [see (6)], which could be eliminated by our triangulation constraint based coregistration method or the NB-method. Thus high-accuracy misregistration estimates are provided.

However, if the difference between the forward and backward looking geometries is large, the flat earth phase and topography phase cannot be canceled out, leading to nonzero residual flat earth phase ($\Delta\phi_{\text{flat}}$) [27] and topography phase ($\Delta\phi_{\text{top}}$).

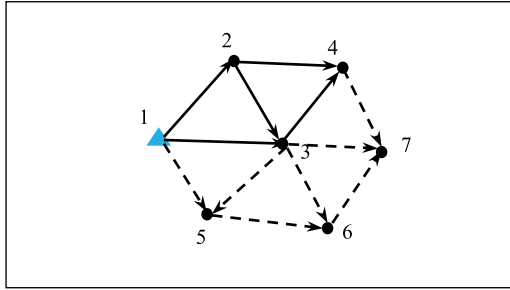


Fig. 6. Example of short-baseline network.

Besides, the possible existing deformation in the azimuth direction would also induce additional signals. Furthermore, the impacts of the ionospheric disturbances and earth tides also can cause additional phase errors, which may not be eliminated by adjustment. Thus, before using the proposed method, we need to correct the geometric difference errors [28], azimuth deformation [8], ionospheric disturbances and earth tides [29].

VI. CONCLUSION

The accuracy of long time-series TOPSAR image coregistration is subject to the coherence of the burst overlap region. To obtain the accuracy of 0.001 pixels for the coregistration of a stack of multitemporal TOPSAR images, as well as newly added images, we first gave a brief review for the existing static methods, including the single master-, temporally transferred-, and network-based methods, for coregistering multitemporal TOPSAR images in this article. Then, we proposed a kinematic coregistration method to coregister newly added TOPSAR images by introducing the SWLSA. The Sentinel-1 TOPSAR images covering Mexico City was selected to test the proposed kinematic method. The results demonstrate that the kinematic method can achieve an accuracy of 0.001 pixels for kinematically coregistering newly added multitemporal TOPSAR images. Compared with the static network-based coregistration method, the proposed method has an improvement of 7% over the static method. And the computational efficiency of kinematic method is significantly higher than the static method. For the big SAR data and the corresponding near real-time processing, our method provides a reference solution.

APPENDIX DESIGN MATRIX CONSTRUCTION

A. Design Matrix for Multitemporal TOPSAR Images Static Coregistration

Given N images, indexing from 1 to N in chronological order, we select the first image (index 1) as the reference for coregistration (it can be any image actually). Then, we construct a network similar to the connections in Fig. 6, and establish the connection matrix \mathbf{G} , with the size of $M \times N$, according to the relationship of image connections. The corresponding connected relation matrix for Fig. 6 is shown in Fig. 7. Because the first phase image is selected as the reference, the design matrix \mathbf{A} of the triangulation chain network is obtained by deleting the corresponding column in matrix \mathbf{G} , namely the design matrix $\mathbf{A} = \mathbf{G}(:, 2 : N)$ with a size of $M \times (N - 1)$. The blue, green,

Design Matrix		Image Index						
		1	2	3	4	5	6	7
Interferometric Pair Index	1	-1	1					
	2		-1	1				
	3	-1		1				
	4			-1	1			
	5		-1		1			
	6	-1				1		
	7			-1		1		
	8			-1			1	
	9			-1				1
	10				-1			1
	11					-1	1	
	12						-1	1

Fig. 7. Example of short-baseline adjustment design matrix. Note: The first column (with grey background) is the reference image that has been deleted.

purple, and orange blocks compose the triangulation adjustment design matrix \mathbf{A} in Fig. 6.

B. Design Matrix for Multitemporal TOPSAR Images Kinematic Coregistration

Given two sets S_1 and S_2 with N_1 and N_2 images, respectively. The images are indexing from 1 to N_1 and $N_1 + 1$ to $N_1 + N_2$. Combining the two sets to construct the short-baseline network in the same way stated in Appendix A, we obtain the overall design matrix \mathbf{A} , with a size of $(M_1 + M_2) \times [(N_1 + N_2) - 1]$. Blocking matrix \mathbf{A} , we obtain the following:

$$\mathbf{A}_1 = \mathbf{A} (1 : M_1, 1 : N_1 - 1)$$

$$\mathbf{B}_1 = \mathbf{A} (1 : M_1, N_1 + 1 : (N_1 + N_2) - 1) = \mathbf{0}$$

$$\mathbf{A}_2 = \mathbf{A} (M_1 + 1 : M_1 + M_2, 1 : N_1 - 1)$$

$$\mathbf{B}_2 = \mathbf{A} (M_1 + 1 : M_1 + M_2, N_1 + 1 : (N_1 + N_2) - 1).$$

For example, there are 7 images in Fig. 6. The first four images compose S_1 , and the rest three images compose S_2 . The short-baseline network of S_1 is denoted by the solid link section, and the expanding network is denoted by the dotted link section. Then, in Fig. 7, the blue, purple, green, and orange blocks correspond to matrix \mathbf{A}_1 , \mathbf{B}_1 (Note: All elements of \mathbf{B}_1 are zero), \mathbf{A}_2 , and \mathbf{B}_2 , respectively.

REFERENCES

- [1] F. De Zan and A. M. Guarnieri, "TOPSAR: Terrain observation by progressive scans," *IEEE Trans. Geosci. Remote Sens.*, vol. 44, no. 9, pp. 2352–2360, Sep. 2006.
- [2] G. Davidson, V. Mantle, B. Rabus, D. Williams, and D. Geudtner, "Implementation of TOPS mode on RADARSAT-2 in support of the Sentinel-1 mission," in *Proc. ESA Living Planet Symp.* 2013, pp. 1–22.
- [3] A. Meta, P. Prats, U. Steinbrecher, J. Mittermayer, and R. Scheiber, "First TOPSAR image and interferometry results with TerraSAR-X," in *Proc. ESA Fringe Workshop*, 2007, pp. 1–8. [Online]. Available: https://elib.dlr.de/53262/1/fringe07_day4_TOPSAR_Meta.pdf, http://earth.esa.int/workshops/fringe07/participants/650/pres_650_meta.pdf
- [4] P. Prats, L. Marotti, S. Wollstadt, and R. Scheiber, "Investigations on TOPS interferometry with TerraSAR-X," in *Proc. IEEE Int. Geosci. Remote Sens. Symp.*, 2010, pp. 2629–2632.

[5] L. Marotti, P. Prats, R. Scheiber, S. Wollstadt, and A. Reigber, "TOPS differential SAR interferometry with TerraSAR-X," in *Proc. ESA Fringe Workshop*, 2011, pp. 1–6.

[6] L. Marotti, P. Prats, R. Scheiber, S. Wollstadt, and A. Reigber, "Differential SAR interferometry with TerraSAR-X TOPS data: Mexico City subsidence results," in *Proc. 9th Eur. Conf. Synthetic Aperture Radar*, 2012, pp. 677–680.

[7] P. Prats-Iraola, R. Scheiber, L. Marotti, S. Wollstadt, and A. Reigber, "TOPS interferometry with TerraSAR-X," *IEEE Trans. Geosci. Remote Sens.*, vol. 50, no. 8, pp. 3179–3188, Aug. 2012.

[8] F. De Zan, P. Prats-Iraola, R. Scheiber, and A. Rucci, "Interferometry with TOPS: Coregistration and azimuth shifts," in *Proc. 10th Eur. Conf. Synthetic Aperture Radar*, 2014, pp. 1–4.

[9] E. Sansosti, P. Berardino, M. Manunta, F. Serafino, and G. Fornaro, "Geometrical SAR image registration," *IEEE Trans. Geosci. Remote Sens.*, vol. 44, no. 10, pp. 2861, Oct. 2006.

[10] N. B. D. Bechor and H. A. Zebker, "Measuring two-dimensional movements using a single InSAR pair," *Geophys. Res. Lett.*, vol. 33, no. 16, 2006, Art. no. L16311, doi: [10.1029/2006GL026883](https://doi.org/10.1029/2006GL026883).

[11] A. Ferretti, C. Prati, and F. Rocca, "Permanent scatterers in SAR interferometry," *IEEE Trans. Geosci. Remote Sens.*, vol. 39, no. 1, pp. 8–20, Jan. 2001.

[12] A. Sowter, M. B. C. Amat, F. Cigna, S. Marsh, A. Athab, and L. Alshammari, "Mexico City land subsidence in 2014–2015 with Sentinel-1 IW TOPS: Results using the Intermittent SBAS (ISBAS) technique," *Int. J. Appl. Earth Observ. Geoinf.*, vol. 52, pp. 230–242, 2016.

[13] F. De Zan and P. Prats-Iraola, "Joint coregistration of SAR images with an application to TerraSAR-X TOPS mode datasets," in *Proc. Living Planet Symp.*, 2013, pp. 1–5.

[14] N. Yague-Martinez, F. D. Zan, and P. Prats-Iraola, "Coregistration of interferometric stacks of Sentinel-1 TOPS data," *IEEE Geosci. Remote Sens. Lett.*, vol. 14, no. 7, pp. 1002–1006, Jul. 2017.

[15] H. Fattahi, P. Agram, and M. Simons, "A network-based enhanced spectral diversity approach for TOPS time-series analysis," *IEEE Trans. Geosci. Remote Sens.*, vol. 55, no. 2, pp. 777–786, Feb. 2017.

[16] A. J. Hooper, "Persistent scatter radar interferometry for crustal deformation studies and modeling of volcanic deformation," Ph.D. dissertation, Stanford Univ., Stanford, CA, USA, 2006.

[17] U. Wegmüller, C. Werner, T. Strozzi, A. Wiesmann, O. Frey, and M. Santoro, "Sentinel-1 support in the GAMMA Software," *Procedia Comput. Sci.*, vol. 100, pp. 1305–1312, 2016.

[18] R. Scheiber and A. Moreira, "Coregistration of interferometric SAR images using spectral diversity," *IEEE Trans. Geosci. Remote Sens.*, vol. 38, no. 5, pp. 2179–2191, Sep. 2000.

[19] B. Xu et al., "Continent-wide 2-D co-seismic deformation of the 2015 Mw 8.3 Illapel, Chile earthquake derived from Sentinel-1A data: Correction of azimuth co-registration error," *Remote Sens.*, vol. 8, no. 5, May 2016, Art. no. 376.

[20] P. A. Rosen et al., "Synthetic aperture radar interferometry," *Proc. IEEE*, vol. 88, no. 3, pp. 333–382, Mar. 2000.

[21] R. F. Hanssen, *Radar Interferometry: Data Interpretation and Error Analysis*. Berlin, Germany: Springer, 2001.

[22] M. Jiang, X. Ding, Z. Li, X. Tian, C. Wang, and W. Zhu, "InSAR coherence estimation for small data sets and its impact on temporal decorrelation extraction," *IEEE Trans. Geosci. Remote Sens.*, vol. 52, no. 10, pp. 6584–6596, Oct. 2014.

[23] Y. Morishita and R. F. Hanssen, "Deformation parameter estimation in low coherence areas using a multisatellite InSAR approach," *IEEE Trans. Geosci. Remote Sens.*, vol. 53, no. 8, pp. 4275–4283, Aug. 2015.

[24] J. Zhu, T. Zuo, and Y. Song, *Error Theory and Basis of Surveying Adjustment*. Beijing, China: Surveying and Mapping Press, 2013.

[25] D. Sandwell, R. Mellors, X. Tong, M. Wei, and P. Wessel, "GMTSAR: An InSAR processing system based on generic mapping tools," Univ. California, San Diego, CA, USA: Library – Scripps Digital Collection. [Online]. Available: <https://escholarship.org/uc/item/8zq2c02m>

[26] R. Torres et al., "GMES Sentinel-1 mission," *Remote Sens. Environ.*, vol. 120, no. 1, pp. 9–24, 2012.

[27] B. Xu, Z. Li, Y. Zhu, J. Shi, and G. Feng, "SAR interferometric baseline refinement based on flat-earth phase without a ground control point," *Remote Sens.*, vol. 12, no. 2, 2020, Art. no. 233.

[28] H. S. Jung, J. S. Won, and S. W. Kim, "An improvement of the performance of multiple-aperture SAR interferometry (MAI)," *IEEE Trans. Geosci. Remote Sens.*, vol. 47, no. 8, pp. 2859–2869, Aug. 2009.

[29] M. Lei, Q. Wang, X. Liu, B. Xu, and H. Zhang, "Influence of ocean tidal loading on InSAR offshore areas deformation monitoring," *Geodesy Geodyn.*, vol. 8, no. 1, pp. 70–76, 2017.



Bing Xu received the B.S. and Ph.D. degrees in geodesy and surveying engineering from Central South University, Hunan, China, in 2011 and 2016, respectively.

From June 2012 to June 2013, he was a Junior Research Assistant with the Institute of Space and Earth Information Science, the Chinese University of Hong Kong, Hong Kong. From June 2013 to January 2014, he was a Research Assistant with the Department of Land Surveying and Geo-Informatics, the Hong Kong Polytechnic University, Hong Kong.

He currently works with the Radar Group at the School of Geoscience and Info-Physics, Central South University, Changsha, China. His research interests include SAR big data processing and algorithm developments for multitemporal InSAR technique.



Zhiwei Li received the bachelor's and master's degrees in surveying engineering from Central South University of Technology (now Central South University), Changsha, China, in 1997 and 1999, respectively, and the Ph.D. degree in remote sensing from The Hong Kong Polytechnic University, Hong Kong, in 2005.

He is currently a Full Professor with the Department of Surveying and Remote Sensing, School of Geosciences and Info-Physics, Central South University. His research interests include interferometric

synthetic aperture radar for mining, permafrost and glacier motion monitoring, especially their 3-D deformation mapping. He has authored or co-authored more than 60 papers in international peer-reviewed journals.



Yan Zhu received the bachelor's degree in surveying and mapping engineering from Central South University, Changsha, China, in 2018.

Since 2018, he has been with Institute of Radar Remote Sensing & Imaging Geodesy (RRSIG), Central South University. His studies regard Interferometric Synthetic Aperture Radar (InSAR). In particular, his main research interests include surface deformation monitoring, SqueeSAR, and the geological application of InSAR.



Jiancun Shi received the B.E. degree in geomatics from Qinghai University, Xining, China, in 2015, and the M.S. degree in surveying science and technology from China University of Geosciences, Beijing, China, in 2018.

She is currently working toward the Ph.D. degree in the Central South University, Changsha, China, with the research interest in monitoring and interpretation of mining areas using InSAR technology and Inversion models.



Guangcai Feng received the master's degree in surveying engineering from Central South University, Changsha, China, in 2006, and the Ph.D. degree in geophysics and geodesy from The Hong Kong Polytechnic University, Hong Kong, in 2011.

He is currently an Associate Professor with the Department of Surveying and Remote Sensing, School of Geoscience and Info-Physics, Central South University. His research interests include interferometric synthetic aperture radar for inverting source parameters of earthquakes and ground deformation monitoring in urban areas.